Determination of Asymmetric Structure of Ganglioside-DPPC Mixed Vesicle Using SANS, SAXS, and DLS

Mitsuhiro Hirai,* Hiroki Iwase,† Tomohiro Hayakawa,* Masaharu Koizumi,* and Hiroshi Takahashi*
*Department of Physics, Gunma University, Maebashi 371-8510, Japan; and †Institute of Materials Structure Science, KEK, 1-1 Oho, Tsukuba 305-0801, Japan

ABSTRACT Functions of mammalian cell membrane microdomains being rich in glycosphingolipids, so-called rafts, are now one of the current hot topics in cell biology from the intimate relation to cell adhesion and signaling. However, little is known about the role of glycosphingolipids in the formation and stability of the domains. By the use of the inverse contrast variation method in small-angle neutron scattering (SANS), combined with small-angle x-ray scattering (SAXS) and dynamic light scattering (DLS), we have determined an asymmetric internal structure of the bilayer of the small unilamellar vesicle (SUV) of monosialoganglioside (G_{M1})-dipalmitoylphosphatidylcholine (DPPC) mixture ([G_{M1}]:[DPPC] = 0.1:1). A direct method using a shell-model fitting with a size distribution function describes consistently all experimental results of SANS, SAXS, and DLS. We have found that G_{M1} molecules predominantly localize at SUV outer surface to form a highly hydrophilic layer which is dehydrated with the rise of temperature from 25°C to 55°C accompanied by the conformational change of the oligosaccharide chains. The average SUV size determined is ~200 Å, which is comparable to the reported value 260 ± 130 Å of glycosphingolipids microdomains. The present results suggest that the preferential asymmetric distribution of gangliosides is essential to define the size and stability of the domains.

INTRODUCTION

Structure and function of mammalian cell membrane domains, so-called rafts, have been attracting a huge interest and are one of the current hot topics in cell biology since these domains are postulated to have a significant function as a molecular device for localization of specific proteins and to be involved in important membrane-associated events such as signal transmission, cell adhesion, and lipid/protein sorting (Simons and Ikonen, 1997; Simons and Toomre, 2000; Hakomori, 2001). A common feature of cell membrane domains is their peculiar lipid composition, being rich in glycosphingolipids (GSLs), sphingomyelin, and cholesterol. GSLs and sphingomyelin organize microdomains with cSrc and Src family kinases (Kasahara et al., 1997, 2000; Harder et al., 1998; Prinetti et al., 2001) and G-proteins (Moffett et al., 2000), which are involved in cell-surface signal transduction. Especially, GSLs are suggested to play an important role in the formation and function of membrane microdomains.

Gangliosides, major components of GSLs, are acidic lipids composed of a ceramide linked to an oligosaccharide chain containing one or more sialic acid residues. Gangliosides are mostly located on the cell-surface membranes in the central nervous system, and are rich in lipid microdomains with other particular lipids and proteins in neuronal cells (Ledeen and Yu 1982; Prinetti et al., 2000). The functionality of GSL microdomains is attributable to a unique feature of GSLs, namely to the presence of hydroxyl- and amido-groups in ceramide moiety, which work as hydrogen bond donors and acceptors. This feature is not shared by glycerophospholipids that work only hydrogen bond acceptors (Pascher, 1976; Ferraretto et al., 1997). Due to this feature and an enrichment of oligosaccharides in hydrophilic moiety, GSLs are assumed to form complex networks of hydrogen bonding between those lipids and water molecules (Ferraretto et al., 1997). Despite the amount of physiological studies of GSL microdomain functions, the direct structural evidence of the formation and functionality of the microdomains is still poor.

Functionality of the GSL microdomains is assumed to be closely relate the peculiar features of ceramide and oligosaccharide portions, therefore, it is particularly interesting and important to elucidate physicochemical characteristics of ganglioside aggregates. By using synchrotron radiation small-angle x-ray scattering (SR-SAXS), small-angle neutron scattering (SANS) and calorimetry, we have reported the structural characteristics of ganglioside micelles depending on temperature (Hirai et al., 1996a, 1996b, 1998a, 1999; Hirai and Takizawa, 1998; Hayakawa and Hirai, 2002), pH and concentration (Hirai et al., 1996c). We have also clarified the binding specificity of gangliosides with proteins depending on the combination of oligosaccharide chain and protein surface modification (Hirai et al., 1995, 1998b). We showed the following results on the thermal structural stability of ganglioside micelles. The elevation of temperature induces a significant shrinkage of the hydrophilic region of the ganglioside micelle at physiological temperature from 20°C to 40°C, indicating that the oligosaccharide chains of ganglioside molecules change those conformations sensitively against the rise of temperature (Hirai et al., 1996a, 1996b, 1998a). This phenomenon accompanies the extrusion of a large amount of water from the hydrophilic region of the

Submitted January 6, 2003, and accepted for publication April 10, 2003.
Address reprint requests to Mitsuhiro Hirai, Dept. of Physics, Gunma University 4-2 Aramaki, Maebashi 371-8510, Japan. Tel.: +81-272-20-7554; Fax: +81-272-20-7551 or 7552, E-mail: mhirai@fs.aramaki.gunma-u.ac.jp.

0006-3495/03/09/1600/11 $2.00

micelles (Hirai and Takizawa, 1998; Hayakawa and Hirai, 2002) and an alteration of the micellar surface charge (Hirai et al., 1999). Moreover, the above characteristics of ganglioside aggregates also showed a great dependency on the variety of oligosaccharide chains. In addition our neutron spin echo (NSE) study shows that the above structural changes of gangliosides significantly affect the micellar dynamics such as bending fluctuation (Hirai et al., 2001). From these previous results, the microdomains enriched in gangliosides are suggested to be able to greatly modulate local charge, hydrophilicity, and dynamics in cell surfaces due to their intrinsic properties, which would regulate directly or indirectly the microdomain functions such as an accumulation of proteins playing roles in transmembrane signaling events and their activation. On the other hand, hydrophilic environments afforded by gangliosides actually have the pivotal role in some protein activity. Maggio and Danniele (Maggio et al., 1994; Daniele et al., 1996) showed that gangliosides have inhibitory effects on phospholipase A_2 and C activities. As phospholipase activity is concurrent with a dehydration process of membrane interfaces (Jain et al., 1988), it is suggested that the high capacity of gangliosides to structure water plays a major role in those inhibitory effects (Arnulphi et al., 1997).

Even structural information of model membrane vesicle containing gangliosides is rather limited. Then, to obtain direct evidence of localization of gangliosides in bilayer membranes and to clarify the thermal stability, we have carried out experiments on monosialoganglioside (G_{M1})-DPPC mixed small unilamellar vesicles (SUVs) as a model raft system. For characterizing the details of the internal structure of the SUVs, we have used three different scattering techniques complementarily, namely, SANS with the inverse contrast variation method (Knoll et al., 1985), SR-SAXS, and DLS. In the SANS inverse contrast variation measurements, under a defined molar ration of $[G_{M1}]/[DPPC]$ we changed the molar ratio between hydrated DPPC and deuterated DPPC to vary the contrast of the vesicle in deuterium oxide solvent. By using this method we have obtained high statistical SANS data of the SUV at four different contrasts. The same samples used for the SANS measurements have been concurrently used for the SAXS and DLS measurements. From these data we have successfully confirmed an asymmetric distribution of gangliosides in the SUV bilayer and determined the bilayer structure. We have also found a thermal structural change which accompanies the dehydration and bending oligosaccharide chain portion at the SUV outer surface.

MATERIALS AND METHODS

Sample preparation

The ganglioside used was monosialoganglioside, G_{M1}, from bovine brain purchased from Sigma Chemical (St. Louis, MO, USA), which was used without further purification. For the employment of the inverse contrast variation method, we used both hydrated and deuterated phospholipids. 1,2-Dipalmitoyl-*sn*-glycero-3-phosphocholine (h-DPPC) and 1,2-dipalmitoyl-d62-*sn*-glycero-3-phosphocholine (d-DPPC) purchased from Avanti Polar Lipids (Alabaster, AL, USA). Ganglioside-DPPC mixed vesicles were prepared according to the method described by Sillerud et al. (1979) with the following modifications. G_{M1}, h-DPPC and d-DPPC were separately dissolved in the chloroform/methanol mixture solvent (1/1 (v/v)). These solutions were mixed with the appropriate molar ratios. After mixing, to remove the organic solvent, the G_{M1}-DPPC mixture solutions were dried under a nitrogen stream and annealed in vacuo overnight at 45°C (above the gel-to-liquid crystal transition temperature of DPPC). The dried mixtures were suspended again in 50 mM Hepes buffer (pH 7.0), warmed to 50°C, and vortexed at 50°C for ~20 min, where the water used was deuterium oxide (99.9+ atom % D) from Aldrich (Milwaukee, WI, USA). For preparing SUV, the mixtures were sonicated for 20 min at 50°C using a high-power probe-type ultrasonicator (Model UH-50 of SMT (Akita, Japan) at 50 W. These sonicated solutions were incubated for 2 hr at 45°C, and kept at 4°C for ~24 hr before scattering measurements. The molar ratio $[G_{M1}]/[DPPC]$ of the mixture was 0.1/1, where the DPPC concentration was fixed at 1% w/v. The molar ratios between h-DPPC and d-DPPC were 1/0, 0.3/0.7, 0.7/0.3, and 0/1. These samples with different [h-DPPC]/[d-DPPC] ratios were served for SANS, SAXS, and DLS experiments. Before scattering measurements the sample solutions were filtered with a membrane filter of 0.1-μm pore size from Whatman (Cambridge, UK).

Neutron, x-ray, and light scattering experiments

Small-angle neutron scattering measurements were carried out by using a SANS spectrometer installed at C1-2 beam port at the research reactor JRR-3M of the Japan Atomic Energy Research Institute (JAERI), Tokai, Japan. The neutron wavelength used was 7.0 Å. The sample to two-dimensional area detector distance was 2 m and 8 m, which covered q-range from 0.005 $Å^{-1}$ to 0.15 $Å^{-1}$. The exposure time was 60 min. Small-angle x-ray scattering measurements were carried out by using a SAXS spectrometer installed at BL-15A beam port of the synchrotron radiation source (PF) at the High Energy Accelerator Research Organization (KEK), Tsukuba, Japan. The x-ray wavelength, the sample-to-detector distance, and the exposure time were 1.49 Å, 190 cm, and 300 s, respectively. For both SANS and SAXS measurements, the temperatures of the samples were controlled at 25°C and 55°C. Dynamic light scattering measurements were carried out by using the DLS spectrometer of Zetasizer 3000 from Malvern Instrument (Worcstershire, UK), which used 10 mW He-Ne laser. The temperatures of the samples were controlled the same as in the SANS and SAXS measurements.

SANS and SAXS data analyses

For SANS data the background scattering was corrected by using the following standard method:

$$I(q) = \left[\frac{I_{\mathrm{sol}}(q)}{M_{\mathrm{sol}}T_{\mathrm{sol}}} - \frac{I_{\mathrm{cell}}(q)}{M_{\mathrm{cell}}T_{\mathrm{cell}}}\right] - \left[\frac{I_{\mathrm{solv}}(q)}{M_{\mathrm{solv}}T_{\mathrm{solv}}} - \frac{I_{\mathrm{cell}}(q)}{M_{\mathrm{cell}}T_{\mathrm{cell}}}\right], \quad (1)$$

where $I_{\mathrm{sol}}(q)$, $I_{\mathrm{solv}}(q)$, and $I_{\mathrm{cell}}(q)$ are the circular averaged scattering data from the solution, the solvent, and the cell, respectively. M and T are the incident neutron beam intensity and the transmission of the solution, the solvent and the cell, respectively. The following data analyses were carried out. The details of the small-angle scattering data analyses were described elsewhere (Hirai et al., 1996a,b). By using the Guinier plot ($\ln I(q)$ vs. q^2) on the data sets in a defined small q range (0.007–0.01 $Å^{-1}$), we determined the values of both zero-angle scattering intensity $I(0)$ and radius of gyration R_g by using the following equation

$$I(q) = I(0)\exp(-q^2R_g^2/3), \quad (2)$$

where $q = (4\pi/\lambda)\sin(\theta/2)$, θ and λ, are the scattering angle and the x-ray

and neutron wavelengths. The distance distribution function $p(r)$ was obtained by the Fourier transform of the observed scattering intensity $I(q)$ as

$$p(r) = \frac{1}{2\pi^2}\int_0^\infty rqI(q)\sin(rq)dq. \quad (3)$$

To calculate the function $p(r)$, the extrapolation for the small-angle data sets was done by using the Guinier plot and the modified intensity,

$$I'(q) = I(q)\exp(-kq^2), \quad (4)$$

(k is the artificial damping factor) was used to remove the Fourier truncation effect. The maximum diameter D_{max} of the particle was estimated from the $p(r)$ function satisfying the condition $p(r) = 0$ for $r > D_{max}$ (Glatter, 1982).

In the present case, The repulsive Coulomb interaction between SUV particles originated from the sialic acid residues of GM1 is week enough to be neglected.

In our previous articles (Hirai et al., 1996c, 1999), we treated a repulsive interaction between disialoganglioside G_{D1} micellar systems, where we used both the interparticle interaction form factor (Hayter and Penfold, 1981) and the shell-model structure factor, and determined both the effective charge and internal structure of the micelles. The effect of the repulsive interaction on the small-angle scattering data was shown to be neglected below 0.5% w/v G_{D1}. G_{D1} has twice of sialic acid residues compared with G_{M1} and the present G_{M1} concentration is ~0.2% w/v. Then, in the present case the effect of the repulsive interaction between the SUVs on the small-angle scattering data can be neglected experimentally, and only the size distribution affects those data. In such a case, the shell-modeling method combined with a size distribution function is applicable to determine both the internal structure and size distribution of the SUVs by fitting the experimental SANS and SAXS scattering curves with the theoretical ones, as shown below. For a polydisperse system composed of particles with an identical shape, the scattering function $I(q)$ is given by

$$I(q) = \int_{R_{min}}^\infty I_s(q,R)D(R)dR, \quad (5)$$

where $D(R)$ is the number distribution function of the particle radius R, and $I_s(q,R)$ is the scattering function of the particle with the radius R. R_{min} is a lower limit of particle radius, namely, in the present case the DPPC bilayer thickness of the SUV. In the present model-fitting analysis, we assume that the SUV particle is composed of multispherical shells. As shown previously (Hirai et al., 1994, 1996a,b), the spherical averaged scattering function $I_s(q,R)$ from an ellipsoidal particle with radius R composed of n shells with different average scattering densities is given by

$$I_s(q,R) = \int_0^1 \left[3\left\{\bar{\rho}_1 V_1 j_1(qR_1)/(qR_1) + \sum_{i=2}^{n}(\bar{\rho}_i - \bar{\rho}_{i-1})V_i j_1(qR_i)/(qR_i)\right\}\right]^2 dx, \quad (6)$$

where $\bar{\rho}_i$ is the average excess scattering density (so-called contrast) of i th shell with a shape of an ellipsoid of rotation, j_1 is the spherical Bessel function of the first rank. R_i is defined as

$$R_i = r_i(1 + x^2(\nu_i^2 - 1))^{1/2}, \quad (7)$$

where r_i and ν_i are the semiaxis and its ratio of ith ellipsoidal shell, respectively. For a spherical-shelled particle ($\nu_i = 1$, $R_i = r_i$), Eq. 4 is simplified as

$$I_s(q,R) = 9\left\{\bar{\rho}_1 V_1 j_1(qR_1)/(qR_1) + \sum_{i=2}^{n}(\bar{\rho}_i - \bar{\rho}_{i-1})V_i j_1(qR_i)/(qR_i)\right\}^2. \quad (8)$$

$\bar{\rho}_i$ and R_i were used as fitting parameters. As a number distribution function of particle radii $D(R)$, we adopted the following Gaussian distribution function which is used in many cases of SUV systems (Balgavy et al., 2001).

$$D(R) = \frac{1}{\sqrt{2\pi}\sigma}\exp\left\{-\frac{(R-\bar{R})}{2\sigma^2}\right\}, \quad (9)$$

where $\bar{R}$ and σ are the average radius and the standard deviation, respectively. By using Eqs. 5, 8, and 9, we can fit the theoretical scattering function to the experimental one from the polydisperse SUV particles, and can determine both the size-distribution function and the bilayer structure of the SUV.

RESULTS AND DISCUSSION

Inverse contrast dependence of scattering curves

Fig. 1 shows the SANS curves $I(q)$ of the SUV samples of $[G_{M1}]/[DPPC] = 0.1/1$ mixture at different inverse contrasts (1% w/v DPPC in D_2O at pH 7), where the molar ratios of [h-DPPC]/[d-DPPC] are 1/0, 0.7/0.3, 0.3/0.7, and 0/1, respectively. Figs. 1 *A* and 1 *B* correspond to $I(q)$ at 25°C and 55°C. The insets in Fig. 1 show the SAXS curves of the same samples used for the SANS measurements. The SANS curve greatly changes depending on the molar ratio of [h-DPPC]/[d-DPPC]. When we use the reported volumes of component groups of phospholipids (Armen et al., 1998; Nagle and Tristram-Nagle, 2000), the average scattering densities of the hydrophobic tail portions of h-DPPC and d-DPPC molecules for neutron can be estimated to be -9.17×10^8 cm^{-2} at L_β phase (-8.27×10^8 cm^{-2} at L_α phase) and 7.73×10^{10} cm^{-2} at L_β (6.99×10^{10} cm^{-2} at L_α phase). The average scattering densities of the hydrophilic head portions of h-DPPC and d-DPPC including glycerol and carbonyls are identical (1.10×10^{10} cm^{-2}). Thus, the [h-DPPC]/[d-DPPC] ratio dependence of the SANS curve is ascribed to the change of the contrast of the hydrophobic tail region of the SUV for neutron. On the other hand, in the insets of Fig. 1 all SAXS curves at the same temperature agree well with each other, indicating that the SUV samples with different [h-DPPC]/[d-DPPC] molar ratios have the same contrast profiles. This is because the head and tail portions of h-DPPC and d-DPPC molecules have the same x-ray scattering densities which are evidently independent on deuteration of DPPC. Alternatively, the variation of [h-DPPC]/[d-DPPC] ratio affects the structure factor and contrast profile of the SUV particle only for neutron and not for x ray. The good agreement of the SAXS curves at the same temperature convinces us that the sample preparation for the inverse contrast variation measurements was done exactly. Thus, we successfully measured the $[G_{M1}]/[DPPC] = 0.1/1$ SUV at five different contrasts, namely, at five different phases (four from neutron, one from x ray). Clearly the difference in SANS and SAXS curves results from the different contrast profiles of the SUV for neutron and for x ray. In general, the scattering function of a solute particle in solution is obtained from the spherical average of the Fourier transform of self-correlation function of the contrast profile, thus, it is not

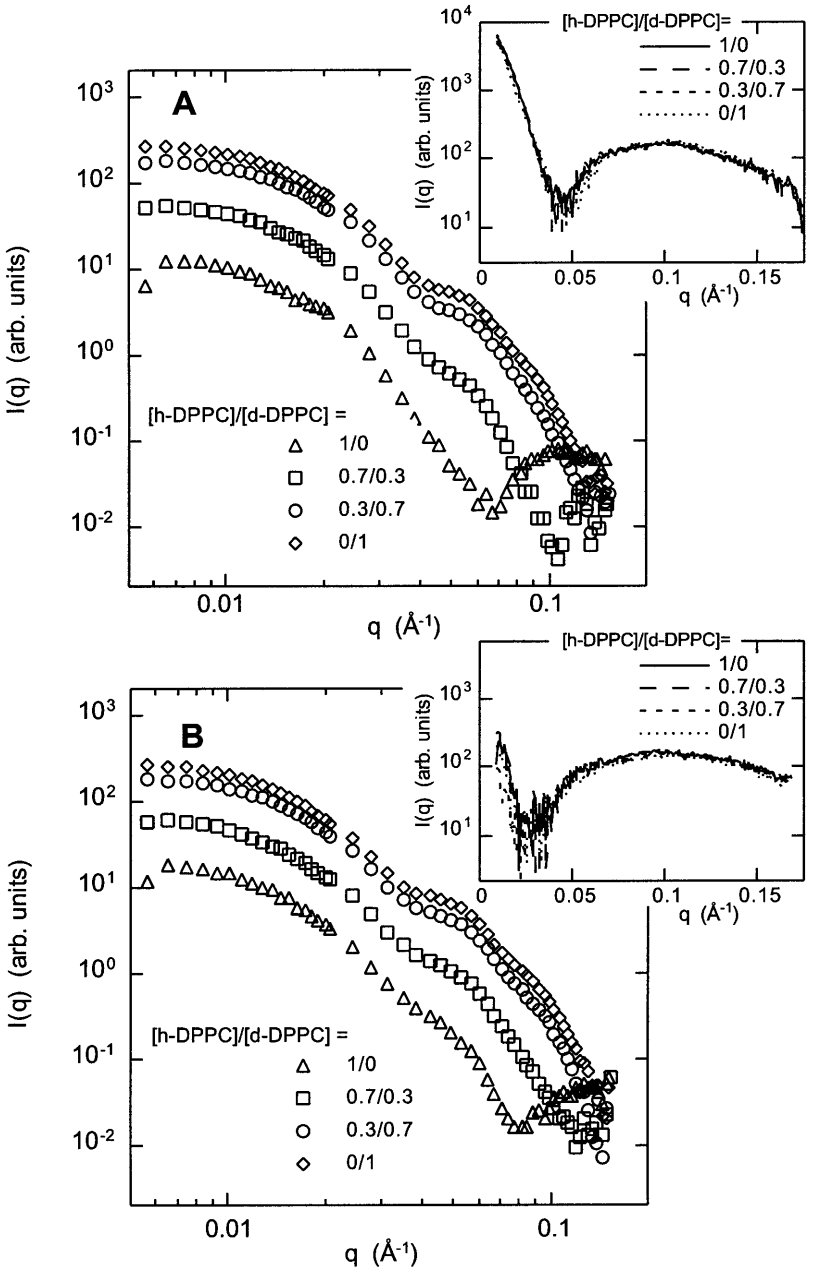

FIGURE 1 SANS curves $I(q)$ of the SUV samples of monosialoganglioside (G_{M1}) and dipalmitoyl phosphocholine (DPPC) mixture ([G_{M1}]/[DPPC] = 0.1/1, 1% w/v DPPC in D_2O at pH 7), where the hydrated- and deuterated-DPPC molar ratio [h-DPPC]/[d-DPPC] varies from 1/0, 0.7/0.3, 0.3/0.7, to 0/1. *A* and *B* correspond to temperatures of 25°C and 55°C. The inset shows the SAXS curves of the same samples used for the SANS measurements at 25°C and 55°C.

appropriate to relate a defined part of the scattering function in reciprocal space to a defined part of the particle structure in real space. However, in the present case, according to the contrast profiles shown below, we can say roughly that the dip and bump in the SAXS curve mostly reflects the bilayer width and that those in the SANS curve (h-DPPC/d-DPPC = 1/0) mostly reflects the width of the hydrophobic region.

Zero-angle scattering intensity and distance distribution function depending on contrast

For a monodisperse solution, the following relation between the contrast and the zero-angle scattering intensity $I(0)$ is well known (Stuhrmann and Miller, 1978).

$$I(0) \propto [(\rho - \rho_s)V]^2 = (\bar{\rho}V)^2, \tag{10}$$

where ρ and ρ_s are the average scattering densities of the solute particle and the solvent, $\bar{\rho}$ and V are the contrast and volume the solute particle, respectively. In the inverse contrast variation method, ρ is a variable changing $\bar{\rho}$. For the case of the SUV, the term $(\rho - \rho_s)V$ is given as follows.

$$(\rho - \rho_s)V = \{\rho_{bilayer}V_{bilayer} + \rho_{core}V_{core}\} - \rho_s V, \tag{11}$$

where $\rho_{bilayer}$, ρ_{core}, $V_{bilayer}$, and V_{core} are the average scattering densities and the volumes of the bilayer and water core regions of the SUV, respectively. As $\rho_{core} = \rho_s$ and $V = V_{bilayer} + V_{core}$ in the present case, Eq. 10 can be rewritten as

$$I(0) \propto [(\rho_{\text{bilayer}} - \rho_s)V_{\text{bilayer}}]^2 = (\bar{\rho}V_{\text{bilayer}})^2. \quad (12)$$

The term of $\rho_{\text{bilayer}}V_{\text{bilayer}}$ is given as

$$\begin{aligned}\rho_{\text{bilayer}}V_{\text{bilayer}} &= N_G\rho_G V_G + N_{\text{DPPC}}\{(1-\alpha)\rho_{\text{h-DPPC}} \\ &\quad + \alpha\rho_{\text{d-DPPC}}\}V_{\text{DPPC}} \\ &= \{N_G\rho_G V_G + N_{\text{DPPC}}\rho_{\text{h-DPPC}}V_{\text{DPPC}}\} \\ &\quad + N_{\text{DPPC}}(\rho_{\text{d-DPPC}} - \rho_{\text{h-DPPC}})V_{\text{DPPC}}\alpha, \quad (13)\end{aligned}$$

where $V_{\text{bilayer}} = N_G V_G + N_{\text{DPPC}}V_{\text{DPPC}}$; N_G, N_{DPPC}, V_G, V_{DPPC}, ρ_G, $\rho_{\text{h-DPPC}}$, and $\rho_{\text{d-DPPC}}$ are the numbers of G_{M1} and DPPC molecules in the SUV, those molecular volumes, and the average scattering densities of G_{M1}, h-DPPC, and d-DPPC molecules, respectively. α is the molar fraction of d-DPPC to the total DPPC content ($0 < \alpha < 1$). For the G_{M1}-DPPC mixed SUV polydisperse solution with the molar ratio of $N_G/N_{\text{DPPC}} = \beta$ ($\beta = 0.1$ in the present case), Eq. 13 of the SUV particle with a size i is given as

$$\begin{aligned}\rho^i_{\text{bilayer}}V^i_{\text{bilayer}} &= N^i_{\text{DPPC}}[\{\beta\rho_G V_G + \rho_{\text{h-DPPC}}V_{\text{DPPC}}\} \\ &\quad + (\rho_{\text{d-DPPC}} - \rho_{\text{h-DPPC}})V_{\text{DPPC}}\alpha]. \quad (14)\end{aligned}$$

Then we can extend Eq. 12 to the case of SUV polydisperse system as follows.

$$\begin{aligned}I(0) \propto \left[\sum_i(\rho^i_{\text{bilayer}} - \rho_s)V^i_{\text{bilayer}}\right]^2 &= \Big[[\{\beta\bar{\rho}_G V_G + \bar{\rho}_{\text{h-DPPC}}V_{\text{DPPC}}\}. \\ &\quad + (\rho_{\text{d-DPPC}} - \rho_{\text{h-DPPC}})V_{\text{DPPC}}\alpha]\sum_i N^i_{\text{DPPC}}\Big]^2, \quad (15)\end{aligned}$$

where ρ^i_{bilayer}, V^i_{bilayer}, and N^i_{DPPC} are the average scattering density, the bilayer volume, and the DPPC molecular number in the SUV with a size i; $\bar{\rho}_G$ and $\bar{\rho}_{\text{h-DPPC}}$ are the contrasts of G_{M1} and h-DPPC molecules, respectively. Thus, the $[I(0)]^{1/2}$ turns out to be simply proportional to the α value even for a polydisperse SUV solution. As the G_{M1} molecule and the head portion of DPPC are not deuterated in the present experiments, the average scattering densities of the SUVs with the different [h-DPPC]/[d-DPPC] ratios for neutron are smaller than that of the deuterated water solvent ($\rho_s = 6.40 \times 10^{10}\,\text{cm}^{-2}$), meaning $\bar{\rho}$ takes negative values for all samples. By extrapolating the Guinier plot ($\ln I(q)$ versus q^2) in Fig. 2 to the intercept, we determined the $I(0)$ values. In Fig. 3 we plot $-[I(0)]^{1/2}$ against the molar fraction of α. The plot in Fig. 3 shows a good linearity and well satisfies Eq. 15. Alternatively, Fig. 3 indicates that the substitutions of h-DPPC for d-DPPC were done appropriately in the present experiments. From this plot we can determine the apparent contrast matching points which are the ρ values satisfying $I(0) = 0$ in α scale, which are 1.27 at 25°C and 1.34 at 55°C. These values correspond to 4.52×10^{10} cm^{-2} and 4.43×10^{10} cm^{-2}, respectively, whereupon we consider the volume change caused by the gel-to-liquid crystal transition of alkyl chains of DPPC (Nagle and Tristram-Nagle, 2000). This means that even by using fully-deuterated DPPC the G_{M1}-DPPC mixed SUV with the molar ratio of $[G_{M1}]/[\text{DPPC}] = 0.1/1$ takes a negative contrast value due to hydrogens brought from G_{M1}.

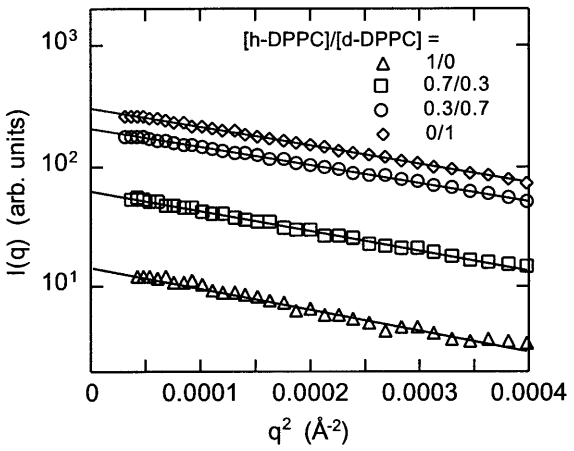

FIGURE 2 Guinier plots ($\ln I(q)$ vs. q^2) in Fig. 1 *A*. The zero-angle scattering intensity $I(0)$ and radius of gyration R_g were determined from these plots in the q-range of 0.007–0.01 Å^{-1}.

Fig. 4 shows the distance distribution functions $p(r)$ obtained from the SANS curves at 25°C by using Eq. 3. From Fig. 4 the maximum diameter D_{max} of the SUV particles was estimated to be ~360 Å. The peak position $p_{\text{max}}(r)$ locates around 115 Å. In the case of a monodisperse solution containing identical hard spherical particles the $p_{\text{max}}(r)$ value simply corresponds to the particle radius. However, as shown by the DLS measurements in the following section, the present SUV solution has an size distribution. Therefore the $p(r)$ function is also given by the summation of the $p(r)$ functions of the solute particles with different sizes. On the other hand the magnitude of $p(r)$ function is proportional to the square of the total scattering amplitude due to the following definition of $p(r)$ function (Glatter, 1982).

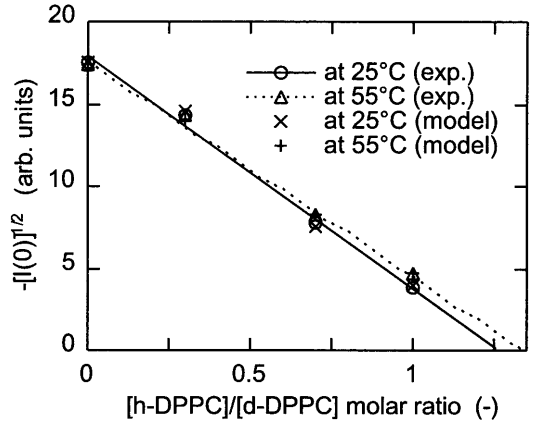

FIGURE 3 Square-root of zero-angle scattering intensity $I(0)$ is plotted against [h-DPPC]/[d-DPPC] ratio. The open marks, ○ and △, correspond to the $I(0)$ values at 25°C and 55°C, respectively. × and + correspond those values obtained from the optimized SUV models with size distributions at different contrasts in Figs. 8 and 9.

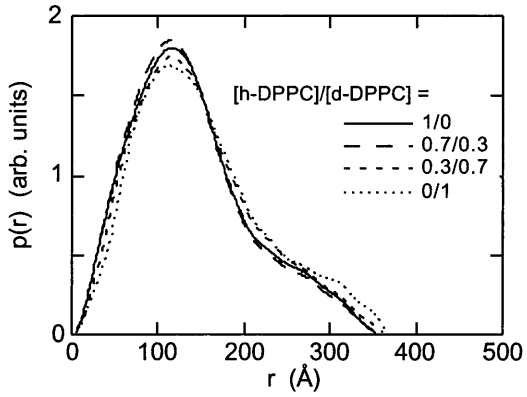

FIGURE 4 Distance distribution functions obtained from SANS curves at 25°C in Fig. 1 *A*.

$$p(r) \equiv r^2\langle \rho(\mathbf{r}) * \rho(-\mathbf{r})\rangle, \quad I(0) = \int_0^{D_{max}} p(r)dr, \qquad (16)$$

where $\rho(\mathbf{r})$ is the scattering density distribution function of a particle, * is the convolution integral, $\langle\ \rangle$ is the average in real space. In addition, the total scattering amplitude is known to be mostly proportional to the molecular weight. Thus in the case of polydisperse system containing spherical particles the $p_{max}(r)$ value is expected to shift to a longer distance compared with the peak position of the $D(R)$ function obtained from DLS measurements. Then the $p_{max}(r)$ value agrees well with the peak position of the $D(R)$ function from the DLS measurement, ~96 Å at 25°C in Fig. 4. Both the $p_{max}(r)$ and D_{max} values were used as initial parameters in the following modeling analyses.

Modeling analyses of SUV internal structure

As shown previously (Hirai et al., 1996a,b, 1998a; Hirai and Takizawa, 1998; Hayakawa and Hirai, 2002), the direct method based on the shell-model fitting analysis using Eq. 6 is very useful to determine internal structures of micellar or vesicular particles. In the present SANS and SAXS we obtained the scattering curves from the same SUV solution at five different phases (four from neutron, one from x ray), and we also measured the number distribution function $D(R)$ of the SUV radius by DLS. Then, by using Eq. 5 we are able to fit the experimental SANS and SAXS scattering curves with the theoretical ones and to determine most appropriate structural parameters of the SUV bilayer that can simultaneously explain all of the experimental scattering curves at five different phases as well as the observed $D(R)$ function.

The scheme of the present modeling analysis is as follows. Due to the maximum diameter of the present SUVs, it is clear that the size distribution of the SUVs affects only the SANS and SAXS data sets in the small-angle region (below $q = \sim 0.025$ Å^{-1}). The internal structure of the SUV depending on contrast mostly appears in the scattering function above $q = \sim 0.03$ Å^{-1}. Then, at the first step we determined the optimized size-distribution function from the SANS and SAXS data below $q = \sim 0.025$ Å^{-1} by using the hard-sphere model fitting with a size distribution. The determined size distribution function agrees well with that measured by DLS as shown below. After the determination of the size distribution function, we executed the internal structure determination of the SUV bilayer by using a shell-model structure factor since the scattering function above $q = \sim 0.03$ Å^{-1} mostly reflects the internal structure of the SUV. For the first approximation, we simplified the SUV structure as a layered sphere composed of four shells, where we considered the inner water-core region and the bilayer composed of three regions, namely one hydrophobic tail region (hydrocarbon chains of G_{M1} and DPPC) sandwiched by two identical hydrophilic head regions (G_{M1} and DPPC heads including the backbones and those hydrated waters). As we knew the size-distribution function and that the most inner shell corresponds to the water core, the fitting parameters were the widths and scattering densities of the head and tail regions. In this fitting process, we used the following criteria based on the geometrical features of G_{M1} and DPPC molecules (Israelachvili et al., 1976). 1), The thickness of the hydrophobic region is shorter than twice the critical chain length of G_{M1} tail (~25 Å). 2), The average scattering density of the hydrophobic region is less than that of L_β (gel) phase (for x ray, $\sim 8.7 \times 10^{10}$ cm^{-2} (Marsh, 1990); $\sim 9.2 \times 10^{10}$ cm^{-2} (Nagle and Tristram-Nagle, 2000)). 3), The thickness of hydrophilic region is longer than the length of DPPC choline head (9.0 ± 1.2 Å) (Büldt et al., 1979; Zaccai et al., 1979; Pabst et al., 2000) and shorter than the extended length of G_{M1} oligosaccharide chain (~22 Å) (McIntosh and Simon, 1994; Hirai et al., 1996a). 4), The average scattering density of this region is less than that of DPPC choline head including glycerol and carbonyls ($\sim 1.2 \times 10^{11}$ cm^{-2} for x ray) (Nagle and Tristram-Nagle, 2000; Balgavy et al., 2001). 5), The SUV radii are larger than the bilayer thickness and smaller than ~200 Å from DLS and $p(r)$ function. Besides the above criteria, in the case of neutron, except for the hydrophobic region the average scattering densities of the other regions take same values at different [h-DPPC]/[d-DPPC] ratios. Under the above criteria, we optimized the model structure to fit the experimental scattering function by the minimization of the reliability factors R defined by $R = \sum|I_{experiment}(q) - I_{model}(q)|/\sum I_{experiment}(q)$. As shown in Fig. 5, the experimental SANS and SAXS scattering curves at the small q region below ~0.03 Å^{-1} seem to be explained to some extent by the optimized model. However, even for the most optimized four-shell model, the theoretical scattering curves show a large deviation from the experimental ones. Such a deviation above $q = \sim 0.04$ Å^{-1} is evidently ascribed to the simplicity of the model structure since the scattering curves at high-q region are much more sensitive to the internal structure of the SUV bilayer.

The average scattering densities and the lengths of G_{M1} and DPPC heads are quit different with each other. Then, at

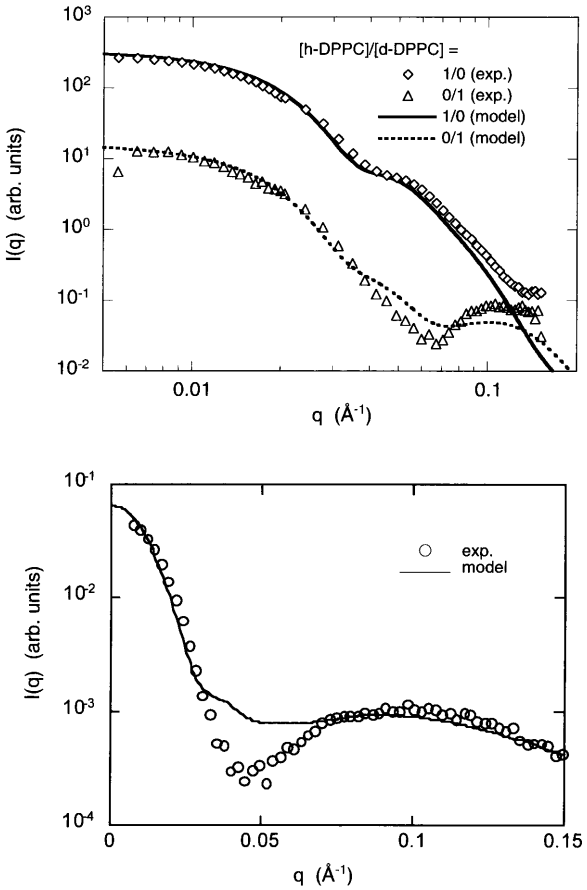

FIGURE 5 Optimized theoretical scattering functions based on SUV model composed of the symmetric four shells with a size distribution. From the SUV outer surface, the constituents of the shells are as follows. 1st and 3rd shells, the hydrophilic G_{M1} and DPPC heads, the glycerol backbones and those hydrated water; 3rd shell, the hydrocarbon chains of DPPC and G_{M1}; 4th shell, water core of the SUV. The experimental SANS and SAXS data in Fig. 1 *A* are also plotted by marks.

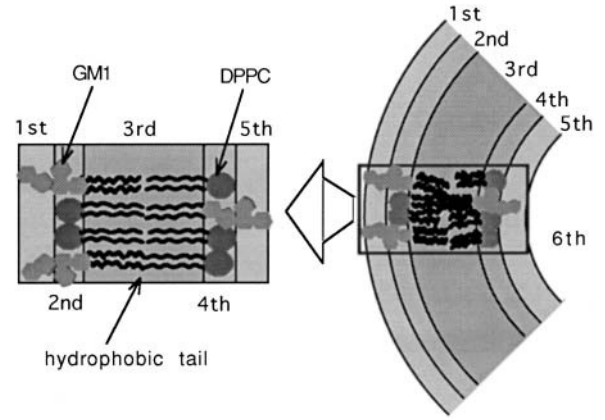

FIGURE 6 Schematic picture of SUV model adopted for the six-shell model fitting. Each shell contains the following constituents. 1st and 5th shells, a part of the oligosaccharide chains protruding from the DPPC choline head surface, hydrated water layer of DPPC choline heads, and penetrated bulk water in these regions; 2nd shell, choline heads, glycerol backbones, and the rest of the oligosaccharide chains; 3rd shell, hydrocarbon chains of DPPC and G_{M1}; 6th shell, water core.

the second approximation, we remodeled the SUV structure as a spherical particle composed of six shells which is schematically shown in Fig. 6. The initial constituents of the six shells from the SUV outer surface are as follows. The first shell contains a portion of the G_{M1} oligosaccharide chains protruding from the DPPC choline head surface, the hydrated-water layer of DPPC choline heads and the bulk water penetrated into this region. The second shell contains the choline heads, the lipid backbones and the rest of the oligosaccharide chains. The third shell corresponds to the hydrocarbon chains of DPPC and G_{M1}. The compositions of the fourth and fifth shells are as same as those of the first and second shells, respectively. The sixth shell is an inner water-core. Here we introduced an additional criterion on the thickness of hydrated-water layer of DPPC choline heads, namely, the thickness of the first hydrated water layer (~3 Å). Based on this model, we have successfully determined the SUV structure which can explain all experimental scattering curves at different phases and the $D(R)$ functions obtained by the DLS measurements at 25°C and 55°C. Fig. 7 shows the experimental scattering curves with the theoretical ones from the best-fitted SUV model at 25°C, where Figs. 7 *A* and 7 *B* correspond to the SANS and SAXS curves, respectively; the inset shows the $D(R)$ functions obtained by the DLS and by the model fittings of SANS and SAXS data. As shown in Fig. 7, all SANS and SAXS scattering curves and the $D(R)$ function from the present experiments are fairly well described by the theoretical ones. Despite the initial model shown in Fig. 6, the model having a symmetric bilayer structure could not explain the scattering curves above $q =$ ~0.03 Å, and the best-fitted model turned to show an asymmetric bilayer structure. The radius values of the maxima in the theoretical $D(R)$ functions are 97.2 Å at 25°C and 102.9 Å at 55°C, which are very close to those experimental values of ~96 Å and ~101 Å. The $I(0)$ values of the best-fitted models, estimated from the Guinier plot in the same q-range used for the experimental data, are in good agreement with the experimental $I(0)$ values, as shown in Fig. 3. The experimental scattering curves and $D(R)$ function at 55°C are also fairly well fitted by the theoretical ones. The reliability factors R in the present fittings for all scattering curves are from 0.02 to 0.09 at 25°C and from 0.05 to 0.11 at 55°C. The errors of the structural parameters obtained are expected to be in same order.

The determined structural parameters of the SUV bilayers at 25°C and 55°C are schematically summarized in Figs. 8 and 9. Fig. 8 shows the contrast distributions in the bilayer, and Fig. 9 shows the thicknesses of the different regions in the bilayer with schematic molecular pictures. In the present modeling analysis using Eq. 8 we can only determine the relative values of the contrast of the shells, therefore, in Fig. 8 the contrast values for both neutron and x ray are tentatively given by normalizing the contrast values of the

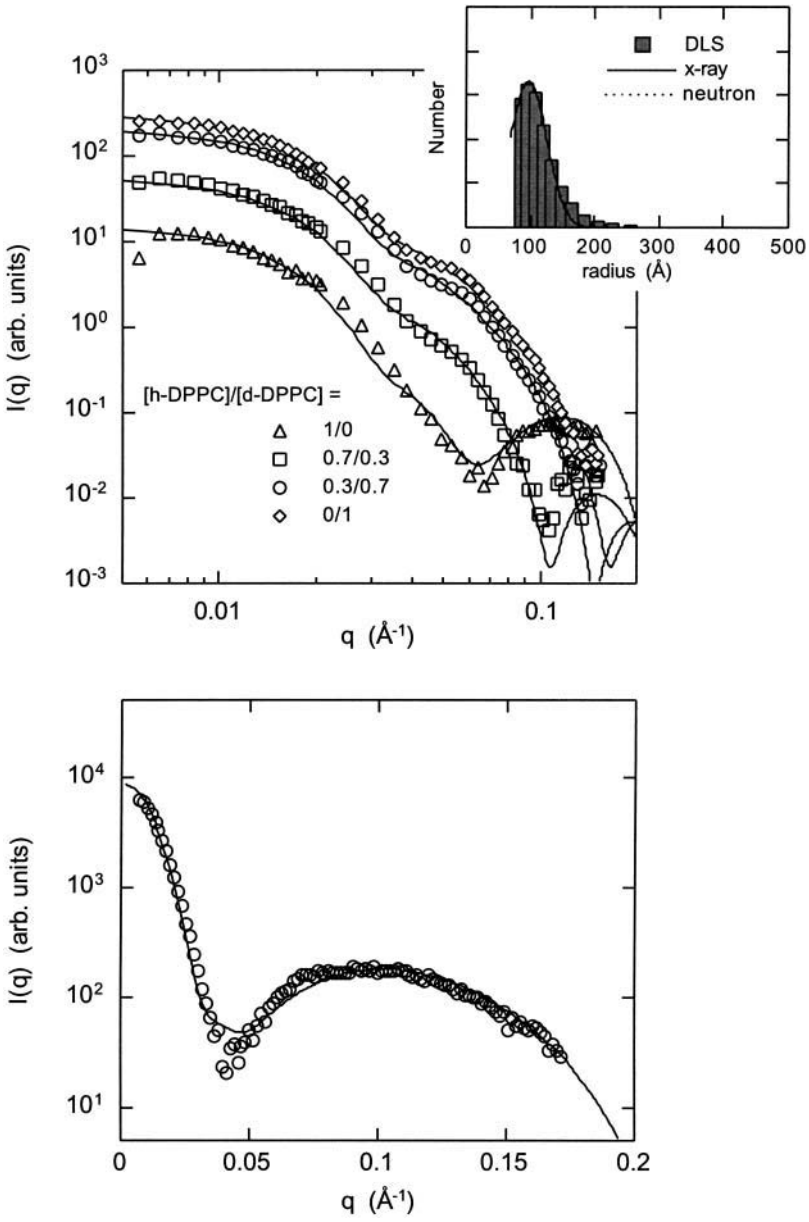

FIGURE 7 Best-fitted theoretical scattering functions with a size distribution at 25°C based on the SUV model in Fig. 6. Experimental SANS, SAXS and DLS data are also shown. *A* and *B* correspond to the SANS and SAXS curves, respectively. The inset shows the number distribution functions of the SUV radius obtained by the DLS and by the model fittings of SANS and SAXS data.

hydrophobic alkyl chain portion at L_β and L_α phases of DPPC. The averaged radius $\bar{R}$ of the SUV at 25°C is 97.2 Å and increases to 102.9 Å at 55°C, which accompanies the enlargement of the average water-core radius from 30.0 Å to 45.1 Å. By the change of temperature from 25°C to 55°C, the thickness of the hydrophobic chain region decreases from 32.9 Å to 26.1 Å, and its contrast decreases for the [h-DPPC]/[d-DPPC] = 0/1, 0.3/0.7, 0.7/0.3 samples in the SANS measurements. These changes are evidently attributable to the chain melting. The thicknesses of the second and the fourth shell regions, mostly corresponding to the choline head group region, are 8.3 Å and 9.3 Å at 25°C, respectively. These values are quite close to the previous experimental values of PC headgroup thickness which were shown by neutron scattering measurements of DPPC bilayers (Büldt et al., 1979; Zaccai et al., 1979) and by wide-angle x-ray scattering measurements of DOPC bilayers (Pabst et al., 2000). The thicknesses of the first, second, and third shells change most evidently due to the rise of temperature from 25°C to 55°C. The total thickness of the first and second shells, corresponding to the hydrophilic outer-surface region of SUV, is 22.2 Å at 25°C. This value is very close to the reported value of 22 Å from G_{M1}/EPC (egg phosphatidylcholine) mixed bilayer (McIntosh and Simon, 1994) at lamellar phase. A recent study of G_{M1}/DPPE (dipalmitoylphosphoethanolamine) monolayer using x-ray reflection also suggests the extended structure of G_{M1} oligosaccharide chains (Majewski et al., 2001). In addition the thickness of the hydrophilic head region of G_{M1} micelle is shown to be ~22 Å at 25°C due to the extended conformation of oligosaccharide chains (Hirai et al., 1996a; Hayakawa and Hirai, 2002). Therefore, the oligosaccharide chains of G_{M1}

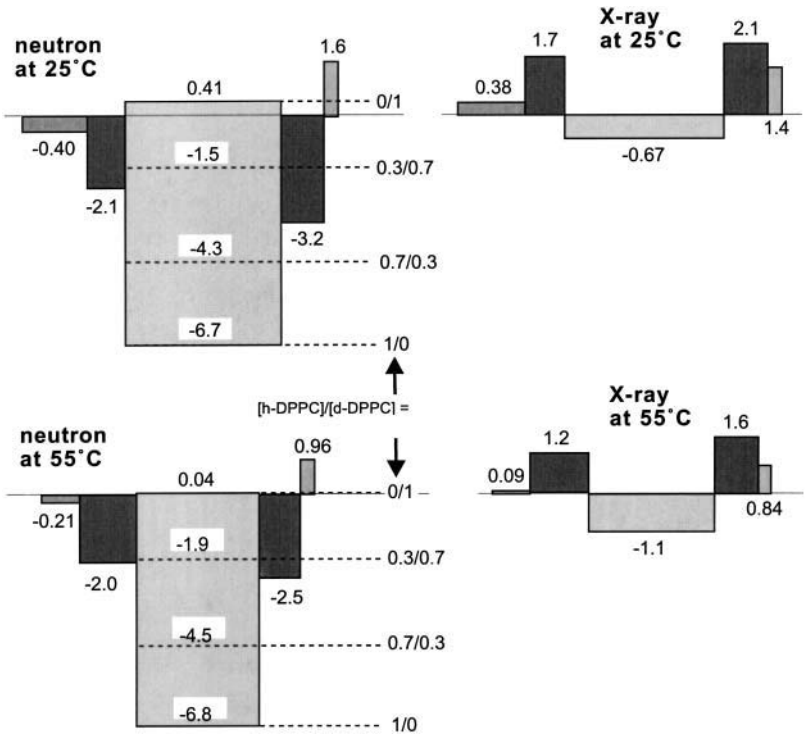

FIGURE 8 Determined contrast distribution profiles of the SUV bilayer structures ($\times 10^{10}$ cm^{-2}) from Fig. 7 for neutron and x ray. The absolute values of the contrasts are tentatively given by the normalization of the contrast values of the hydrophobic tail portion to those estimated at L_β and L_α phases of DPPC.

molecules are understood to take extended conformations on the SUV outer surface. With elevating temperature, the first shell thickness decreases from 13.9 Å to 7.9 Å, and the second shell thickness increases from 8.3 Å to 13.3 Å, whereupon the absolute value of the contrast of the first shell becomes to be small for both neutron and x ray. These changes suggest the bending and dehydration of the oligosaccharide chains as same as the G_{M1} micellar case on temperature elevation (Hirai et al., 1996a; Hayakawa and Hirai, 2002). Evidently, such a bending results in the increase of the second shell thickness.

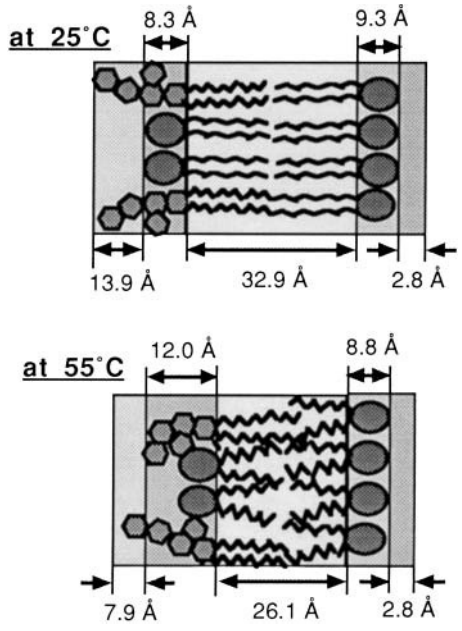

FIGURE 9 Determined thickness of each shell in the SUV bilayer structure from Fig. 7 with schematic pictures of G_{M1} and DPPC molecules.

As we determined the outer and inner radii of the hydrophobic region, we can tentatively estimate the molar ratio of DPPC between the outer and inner surfaces on the assumption that only G_{M1} molecules localize at the SUV outer surface, whereupon we use the following values. The surface area S_g of G_{M1} is ~99 Å^2 and its volume of hydrophobic portion v_g, 1029 Å^3 (Hirai et al., 1996a). The volume of hydrophobic portion of DPPC v_d is 825 Å^3 at L_β phase and 913 Å^3 at L_α phase (Nagle and Tristram-Nagle, 2000). According to the geometrical packing consideration of vesicular particle (Israelachvili et al., 1976), we can simply derive the following relations.

$$N(\alpha v_g + v_d) = 4\pi(R_o^3 - R_i^3)/3 \tag{17}$$

$$\beta N S_d = 4\pi R_i^2 \tag{18}$$

$$\frac{\alpha S_g + (1-\beta)S_d}{\beta S_d} = (R_o/R_i)^2, \tag{19}$$

where R_o and R_i are the outer and inner radii of the hydrophobic region; N, the total number of DPPC in the SUV; α, the molar fraction of [GM1]/[DPPC]; β, the molar fraction of DPPC at the outer and inner surfaces; v_g, v_d, S_g, and S_d are the volumes of hydrophobic portions and the surface areas of G_{M1} and DPPC, respectively. By using Eqs. 17–19, both β and S_d values can be deduced. The β and S_d values are 0.297 and 47.8 Å^2 at 25°C, and 0.372 and 67.6 Å^2,

respectively. The increase of β well explains the decrease of the SUV curvature by the temperature change. In addition the estimated S_d values are in good agreement with the reported ones, 47.9 $Å^2$ at L_β and 64 $Å^2$ at L_β (Nagle and Tristram-Nagle, 2000). Thus, the above estimations also support the preferential localization of G_{M1} molecules at the outer SUV surface as shown by the six-shell modeling analysis.

CONCLUSION

We can conclude the present results as follows. By using both the SAXS method and the inverse-contrast variation SANS method, we successfully observed the scattering curves at four different phases (contrasts). On the basis of the shell modeling method that takes into account of the size distribution of the SUV, we explained very well all experimental scattering curves and size-distribution functions with the theoretical ones. We determined the asymmetric internal structures of the bilayers of the SUVs of G_{M1}-DPPC mixture at 25°C and 55°C. The G_{M1} molecules predominantly locate at the outer surface of the SUV and those oligosaccharide chains take extended conformations at 25°C. The outer-surface layer of the SUV consists of the oligosaccharide chains protruding from the PC head group surface, therefore this layer would be very hydrophilic. The appearance of the asymmetric distribution of G_{M1} molecules is essentially ascribed to the critical packing parameter, ~0.36 obtained from the previous study (Hirai et al., 1996a), of G_{M1} molecule, and would be attributable to the repulsive interaction between the negatively charged bulky headgroups of G_{M1} molecules. These bulky hydrophilic headgroups and their attracted water would require a large surface area to host them in the hydrophilic layer of the membrane. The larger the interfacial area, the stronger the membrane curvature, the more evident the asymmetric distribution of G_{M1} molecules in the membrane. By the temperature rise from 25°C to 55°C, the thickness of the hydrophobic region of the bilayer shrinks in ~6.8 Å by the chain melting transition, whereupon the hydrophilic surface layer collapses by the dehydration and bending of the oligosaccharide chains. The inner surface of the SUV mostly consisting of DPPC choline heads are found to be covered by the high-density hydrated-water layer as similar as other biological molecules (Svergun et al., 1998). This high-density water shell tended to collapse with the temperature elevation.

The asymmetric structure of the SUV containing G_{M1} may not necessarily expand to the case of a large unilamellar vesicle (LUV). According to our DLS measurements, ganglioside mixed LUVs are highly polydisperse and not appropriate for SANS and SAXS experiments followed by detailed modeling analyses. Nevertheless, the presence of huge bulky sugar heads would ensure the preferential localization of gangliosides at outer leaflet of LUV to minimize a bending elastic energy of membrane and to give a positive spontaneous curvature of LUV. According to the reported values of the hydrophobic portion volume and surface area of DPPC (Nagle and Tristram-Nagle, 2000), the so-called critical radius of DPPC vesicle is estimated to be 103 Å at 20°C and 63 Å at 50°C (Israelachvili et al., 1976). However, in the present study we have found that both the asymmetric distribution of G_{M1} and the vesicle size mostly hold against the temperature change from 25°C to 55°C, and the size of the SUV would correspond to a critical size for $[G_{M1}]/[DPPC] = 0.1/1$ mixture. Although the size of the ganglioside-containing SUV would depend on both lipid components and those molar ratios, it is evident that the asymmetric distribution of gangliosides defines the size (curvature) and stability of the SUV against temperature elevation.

On the other hand, recent studies suggest that the size of the GSLs microdomains is ~260 ± 130 Å and that its lifetime is fairly long, on order of minutes (Simons and Toomre, 2000; Pralle et al., 2000). Although the above studies treated native GSLs microdomains, it should be noted that the average diameter of the SUV determined in the present study is ~200 Å which is close to the above reported value. The role of glycosphingolipids in the formation of GSLs domain is considered that physicochemical characteristics of glycosphingolipids supply a driving force inducing spontaneous glycolipid segregation at membrane outer surface to form core domains around which other molecules can gather, forming a more complex GSLs domain (Masserini et al., 2001). Then, combined with the present findings on the SUV structure, we can consider that the preferential asymmetric distribution of gangliosides at the membrane outer surface plays an essential role to form stable core clusters assisting the formation of further complex GSLs domains. This would relate to the long lifetime of the microdomains. In addition, due to the predominant localization of gangliosides at the membrane outer surface, gangliosides can sensitively change those conformations and greatly modulate a hydrophilicity of a cell surface to extracellular stimuli. As mentioned in the introduction section, interaction between GSLs microdomain and some proteins involved in cell-surface signal transductions would be greatly affected by the change of hydrated water on membrane surface (Maggio et al., 1994; Daniele et al., 1996; Jain et al., 1988; Arnulphi et al., 1997). Then, the structural features of ganglioside-containing SUVs found in the present study would suggest an intrinsic role of gangliosides in GSLs domain formation and affinity to a given protein in various signal transductions meditated by biomembrane.

This work was performed under the approval of the Photon Factory Program Advisory Committee of the High Energy Accelerator Research Organization (KEK) (Proposal No. 2000G148) and under the approval of the Neutron Scattering Program Advisory Committee (NSPAC) (Proposal No. 00.027 and 01-024).

REFERENCES

Armen, R. S., O. D. Uitto, and S. E. Feller. 1998. Phospholipid component volumes: determination and application to bilayer calculation. *Biophys. J.* 75:734–744.

Arnulphi, C., P. R. Levstein, M. E. Ramia, C. A. Martin, and G. D. Fidelio. 1997. Ganglioside hydration study by 2H-NMR: dependence on temperature and water/lipid ratio. *J. Lipid Res.* 38:1412–1420.

Balgavy, P., M. Dubnickova, N. Kucerka, M. A. Kiselev, S. P. Yaradaikin, and D. Uhrikova. 2001. Bilayer thickness and lipid interface area in unilamellar extruded 1,2-diacylphosphatidylcholine liposomes: a small-angle neutron scattering study. *Biochim. Biophys. Acta.* 1512:40–52.

Büldt, G., G. J. Seelig, and G. Zaccai. 1979. Neutron diffraction studies on phosphatidylcholine model membrane. I. Head group conformation. *J. Mol. Biol.* 134:673–691.

Daniele, J. J., B. Maggio, I. D. Bianco, F. M. Goni, A. Alonso, and G. D. Fidelio. 1996. Inhibition by gangliosides of Bacillus cereus phospholipase C activity against monolayers, micelles and bilayer vesicles. *Eur. J. Biochem.* 239:105–110.

Ferraretto, A., M. Pitto, P. Palestini, and M. Masserini. 1997. Lipid domains in the membrane: thermotropic properties of sphingomyelin vesicles containing GM1 ganglioside and cholesterol. *Biochemistry.* 36:9232–9236.

Glatter, O. 1982. Data treatment. *In* Small Angle X-ray Scattering. O. Glatter and O. Kratky Editors. Academic Press, London. 119–196.

Hakomori, S. 2001. Membrane microdomains defining cell adhesion and signaling. *Trends Glycosci. Glycotechnol.* 13:219–230.

Harder, T., P. Scheiffele, P. Verkade, and K. Simons. 1998. Lipid domain structure of the plasma membrane revealed by patching of membrane components. *J. Cell Biol.* 141:929–942.

Hayter, J. B., and J. Penfold. 1981. An analytic structure factor for macroion solutions. *Molec. Phys.* 42:109–118.

Hirai, M., T. Hirai, and T. Ueki. 1994. Growing process of scattering density fluctuation of a medium distance in hydrogel of poly (vinyl-alcohol) under stretching. *Macromolecules.* 27:1003–1006.

Hirai, M., T. Takizawa, S. Yabuki, Y. Nakata, H. Mitomo, T. Hirai, S. Shimizu, M. Furusaka, K. Kobayashi, and K. Hayashi. 1995. Complexes of gangliosides with proteins in solution. *Physica B.* 213:751–753.

Hirai, M., T. Takizawa, S. Yabuki, Y. Nakata, and K. Hayashi. 1996a. Thremotropic phase behavior and stability of monosialoganglioside micelles in aqueous solution. *Biophys. J.* 70:1761–1768.

Hirai, M., T. Takizawa, S. Yabuki, T. Hirai, and K. Hayashi. 1996b. Thermotropic structural change of disialoganglioside micelles studied by using synchrotron radiation small-angle x-ray scattering. *J. Phys. Chem.* 100:11675–11680.

Hirai, M., T. Takizawa, S. Yabuki, and K. Hayashi. 1996c. Intermicellar interaction of ganglioside aggregates and structural stability on pH variation. *J. Chem. Soc. Faraday Trans.* 92:4533–4540.

Hirai, M., S. Arai, T. Takizawa, S. Yabuki, and Y. Nakata. 1998a. Characteristics of thermotropic phase transition of glycosphingolipid (Ganglioside) aggregates in aqueous solution. *Thermochim. Acta.* 308:93–99.

Hirai, M., and T. Takizawa. 1998. Intensive extrusion and occlusion of water in ganglioside micelles with thermal reversibility. *Biophys. J.* 74: 3010–3014.

Hirai, M., H. Iwase, S. Arai, T. Takizawa, and K. Hayashi. 1998b. Interaction of gangliosides with proteins depending on oligosaccharide chain and protein surface modification. *Biophys. J.* 74:1380–1387.

Hirai, M., H. Iwase, and T. Hayakawa. 1999. Thermal induced modulation of surface charge of sialoglycosphingolipid micelles. *J. Phys. Chem. B.* 103:10136–10142.

Hirai, M., H. Iwase, and T. Hayakawa. 2001. Structure and dynamics of glycosphingolipid micelles. *J. Phys. Soc. Jpn.* 70:420–423.

Hayakawa, T., and M. Hirai. 2002. Hydration and thermal reversibility of glycolipids depending on sugar-chains. *Eur. Biophys. J.* 31:62–72.

Israelachvili, J. N., D. J. Mitchell, and B. W. Ninham. 1976. Theory of self-assembly of hydrocarbon amphiphiles into micelles and bilayers. *J. Chem. Soc. Faraday Trans. II.* 72:1525–1568.

Jain, M. K., J. Rogers, and G. H. DeHaas. 1988. Kinetics of binding of phospholipase A_2 to lipid/water interfaces and its relationship to interfacial activation. *Biochim. Biophys. Acta.* 940:51–62.

Kasahara, K., K. Watanabe, T. Yamamoto, and Y. Sanai. 1997. Association of Src family tyrosine kinase Lyn with ganglioside GD3 in rat brain. Possible regulation of Lyn by glycosphingolipid in caveolae-like domains. *J. Biol. Chem.* 272:29947–29953.

Kasahara, K., K. Watanabe, K. Takeuchi, H. Kaneko, A. Oohira, T. Yamamoto, and Y. Sanai. 2000. Involvement of gangliosides in glycosylphosphatidylinositol-anchored neuronal cell adhesion molecule TAG-1 signaling in lipid rafts. *J. Biol. Chem.* 275:34701–34709.

Knoll, W., G. Schmidt, and K. Ibel. 1985. The inverse contrast variation in small-angle neutron scattering: a sensitive technique for the evaluation of lipid phase diagrams. *J. Appl. Crystallogr.* 18:65–70.

Ledeen, R. W., and R. K. Yu. 1982. Gangliosides: Structure, isolation, and analysis. *Methods Enzymol.* 83:139–191.

Maggio, B., I. D. Bianco, G. G. Montich, G. D. Fidelio, and R. K. Yu. 1994. Regulation by gangliosides and sulfatides of phospholipase A2 activity against dipalmitoyl-and dilauroyl- phosphatidylcholine in small unilamellar bilayer vesicles and mixed monolayers. *Biochim. Biophys. Acta.* 1190:137–148.

Majewski, J., T. L. Kuhl, K. Kjaer, and G. S. Smith. 2001. Packing of ganglioside-phospholipid monolayers: An x-ray diffraction and reflectivity study. *Biophys. J.* 81:2707–2715.

Marsh, D. 1990. *In* CRC Handbook of Lipid Bilayers. CRC Press, 185–197.

Masserini, M., D. Ravasi, and S. Sonnino. 2001. Role of glycosphingolipids in formation and function of membrane microdomains. *Trends Glycosci. Glycotechnol.* 13:239–250.

Moffett, S., D. A. Brown, and M. E. Linder. 2000. Lipid-dependent targeting of G proteins into rafts. *J. Biol. Chem.* 275:2191–2198.

McIntosh, T. J., and S. A. Simon. 1994. Long- and short-range interactions between phospholipid/ganglioside GM1 bilayers. *Biochemistry.* 33: 10477–10486.

Nagle, J. F., and S. Tristram-Nagle. 2000. Strcuture of lipid bilayers. *Biochim. Biophys. Acta.* 1512:159–195.

Pabst, G., M. Rappolt, H. Amenitsch, and P. Laggner. 2000. Structural information from multilamellar liposomes at full hydration: Full q-range fitting with high quality x-ray data. *Phys. Rev. E.* 62:4000–4009.

Pascher, I. 1976. Molecular arrangements in sphingolipids. Conformation and hydrogen bonding of ceramide and their implication on membrane stability and permeability. *Biochim. Biophys. Acta.* 455:433–451.

Pralle, A., P. Keller, E. L. Florin, K. Simons, and J. K. H. Hörber. 2000. Sphigolipid-cholesterol rafts diffuse as small entities in the plasma membrane of mammalian cells. *J. Cell Biol.* 148:997–1007.

Prinetti, A., V. Chigorno, G. Tettamanti, and S. Sonnino. 2000. Sphingolipid-enriched membrane domains from rat cerebellar granule cells differentiated in culture. *J. Biol. Chem.* 275:11658–11665.

Prinetti, A., S. Prioni, V. Chigorno, D. Karagogeos, G. Tettamanti, and S. Sonnino. 2001. Immunoseparation of sphingolipid-enriched membrane domains enriched in Src family protein tyrosine kinases and in the neuronal adhesion molecule TAG-1 by anti-GD3 ganglioside monoclonal antibody. *J. Neurochem.* 78:1162–1167.

Sillerud, L. O., D. E. Schafer, R. K. Yu, and W. H. Konigsberg. 1979. Calorimetric properties of mixtues of ganglioisde GM1 and dipalmitoylphosphatidylcholine. *J. Biol. Chem.* 254:10876–10880.

Simons, K., and E. Ikonen. 1997. Functional rafts in cell membranes. *Nature.* 387:569–572.

Simons, K., and D. Toomre. 2000. Lipid rafts and signal transduction. *Nat. Rev. Mol. Cell Biol.* 1:31–39.

Stuhrmann, H. B., and A. Miller. 1978. Small-angle scattering of biological structures. *J. Appl. Crystallogr.* 11:325–345.

Svergun, D. I., S. Richard, M. J. H. Koch, Z. Sayers, S. Kuprin, and G. Zaccai. 1998. Protein hydration in solution: experimental observation by x-ray and neutron scattering. *Proc. Natl. Acad. Sci. USA.* 95:2267–2272.

Zaccai, G., G. Büldt, A. Seeling, and J. Seeling. 1979. Neutron diffraction studies on phosphatidylcholine model membrane. II Chain conformation and segmental disorder. *J. Mol. Biol.* 134:693–706.